Journal of Physics:
Conference Series

PAPER • **OPEN ACCESS**

How does wall modeling impact the momentum transfer of modeled wall turbulence?

To cite this article: Xinyi Huang 2026 *J. Phys.: Conf. Ser.* **3230** 012023

How does wall modeling impact the momentum transfer of modeled wall turbulence?

Xinyi Huang[1,2]

[1]Graduate Aerospace Laboratory, California Institute of Technology, Pasadena, USA
[2]Department of Earth, Environment & Planetary Sciences, Brown University, Providence, USA

E-mail: xinyih@brown.edu

Abstract.

Wall-modeled large-eddy simulation (LES) is a cost-effective tool for simulating the wall-bounded turbulence. However, the physics of modeled wall turbulence remains unclear, and thus, the development of a wall model is case-specific. The goal of this work is to explore the physical capability of a wall model, which could potentially explain the generalizability of a wall model. Therefore, the study begins by examining the linear approximation of a wall model and discussing its prediction of the mean profiles at the matching point. Both the *a priori* and the *a posteriori* tests are conducted. The flow behavior is then further explored by decomposing the momentum transfer to investigate its extended impact beyond the matching point. The interaction between a wall model and the LES solver is crucial for accurately predicting the entire profile. Here, special attention is given to the momentum-transfer structures that dominate DNS channel flows, i.e., Qs events. The results show that Qs events are not well captured by wall-modeled LES, particularly the wall-attached events. Based on these observations, potential methods for extending the capability of wall-modeled LES are proposed.

1 Introduction

As a chaotic behavior, turbulence is often characterized through statistical approaches. Direct numerical simulations (DNS) are considered accurate representations of the turbulent systems statistically. However, the computational cost of DNS is not affordable for most real-world applications, especially when a wall is present [1]. To reduce the computational cost, large-eddy simulations (LES) are used, along with wall models for wall-bounded flows, and they are expected to represent the DNS solutions projected onto a lower-dimension system [2]. However, in reality, both the LES and the wall model use models, and their solutions may not reside in the same solution space as the projected DNS.

The modeled wall turbulence in a wall-modeled LES is rarely studied [3]. The development of a wall model is usually case-specific, depending on factors such as rotation, a non-zero pressure gradient, three dimensionality, and flow separation [4–7], etc. The developed model typically has a limited application range and its performance heavily relies on the numerical scheme and the model realization. For example, even when the wall-shear stress is explicitly assigned by using the high-fidelity numerical simulation, the subgrid-scale (SGS) stress model still makes a significant difference in key statistics, such as separation bubble size for a separated flow [8]. This is due to the strong coupling between the SGS model and the wall model within a wall-modeled LES. The coupling is especially complicated with complex physics, which involves the history effect [9, 10]. As the flow develops, it can extend well beyond the designed application range and fail [5]. For example, the equilibrium wall model, which is based on the equilibrium assumption of the near-wall behavior, easily fails when complex flow physics are involved [11], yet it is still the most widely used wall model to begin with [12, 13].

Efforts have been made to extend the applicable range of wall models. Wall models are standardized to ensure reliable performance for canonical flows. The grid requirements of the wall-modeled LES are discussed, and multiple tests are carried out for several validation cases [**?**]. Wall models have also been developed for other real-world scenarios, including compressible flows, flows with a pressure gradient, flows with strong rotation effects and flows in complex geometries [14, 15]. Improvements on wall modeling are also considered for the multi-physics effects, where the multiple physical processes can be combined using a linear assumption along with several building blocks for each fundamental process with the assistance of machine learning techniques [16].

Despite efforts to develop the wall model for increasingly complex physics, the lack of understanding of the modeled wall turbulence in a wall-modeled LES hinders the effective utilization of these models. Traditionally, the success of a wall model is measured by examining the mean velocity profile in the region above the wall-model matching point and below the outer layer in the thin boundary layer [17]. Wall models developed for specific scenarios are usually considered successful when they predict the mean velocity profile without fully understanding the underlying physics. Therefore, high-order statistics, such as Reynolds stress and statistics in the inner boundary layer, are not informative and seldom align with the high-resolution data in experiments [18].

Typically, one fundamental physical assumption of wall modeling is that the instantaneous velocity profiles in the wall unit closely follow the mean velocity profile independently at each location, which in turn provides the same mean velocity profile after coupling with the SGS model in an LES solver. Therefore, an instantaneous local relationship is assumed to exist between the wall shear stress τ_w and the wall-parallel velocity $u_{\parallel,\mathrm{wm}}$ at the matching point location h_{wm}, so that the near-wall momentum transfer can provide an accurate mean velocity $\overline{u}_{\parallel,\mathrm{wm}}$, especially in the streamwise direction. There are two major concerns with the prescribed relationship. First, the combination of the mean velocity profile in the local wall unit, which varies spatially, is essentially a nonlinear combination of the momentum transfer. This was considered to possibly be fixed by filtering the near-wall velocity [19]. Additionally, the self-similar behavior of the instantaneously imposed wall modeled relationship between the near-wall stress τ_w and the wall-parallel velocity $u_{\parallel,\mathrm{wm}}$ unavoidably neglects the impact of coherent structures, which might potentially change the pattern of the momentum transfer.

To understand how the modeled turbulence differs from the original turbulent systems in a wall-model scenario, I will examine the change in the probability density function (p.d.f.) due to the wall model in *a priori* tests in Sec. 2.1. Next, I will discuss the numerical details of the *a posteriori* tests and the corresponding differences from the *a priori* tests in Sec. 2.2. The momentum transfer in a wall-modeled LES will then be decomposed in Sec. 2.3 to understand how modeling provides an accurate profile. The quantification of the momentum-transfer structures will be further analyzed to understand the modeled near-wall behavior from a physical viewpoint in Sec. 3. Finally, the results will be summarized and possible future work is discussed in Sec. 4.

In this work, two of the most commonly used wall-stress models are discussed, i.e. the algebraic wall model, and the ordinary-differential-equation (ODE) equilibrium wall model [14]. Both models are widely used and verified in the wall-modeled LES [15]. They will provide an injective function between $\tau_w/\tau_{w,g}$ and $u_{\parallel,\mathrm{wm}}/u_{\tau,g}$ during implementation, where $\tau_{w,g}$ represents the global wall shear stress and $u_{\tau,g}$ represents the global friction velocity. I use the subscript 'wm' to indicate wall-modeled quantities and the subscript 'g' to indicate global quantities. The modeled wall shear stress is then used as the boundary condition at the wall for the SGS model to complete the turbulence closure.

2 Wall-modeled large-eddy simulations

Wall modeling is typically case-specific because its physical capability is not well understood. The lack of physical knowledge is partly due to the complexity of the interaction between the wall model and the SGS model within the LES solver. The physical behavior concluded from high-resolution data and used for model development is not necessarily the same as in the LES simulations, i.e., the *a posteriori* tests. Therefore, I carry out both *a priori* and *a posteriori* tests to understand the direct impact of a wall model and the coupling between the wall model and the LES solver. The interaction will be further discussed with the help of the momentum transfer equation.

2.1 A priori test of a wall model

In an LES with an under-resolved near-wall grid, a wall model of the wall-stress type is intended to provide the wall shear stress τ_w based on the wall-parallel velocity $u_{\parallel,\mathrm{wm}}$ at the fixed matching location

$h_{\rm wm}$ [14]. Other types of wall models are not the focus of this work, but are discussed later. Here, the flow is in the streamwise direction, without the complication of flow direction due to geometry or the Coriolis effect. To have the statistics of the turbulence perfectly represented by a wall-modeled LES, the p.d.f. of the wall shear stress and the velocity should match its equivalent in the high-resolution solutions after the wall model is applied. In the *a priori* tests, I use the DNS solutions from the Johns Hopkins Database as the high-resolution solutions [20]. To be exact, after applying the wall model function $\tau_w/\tau_{w,g} = g(u_{\|,\rm wm}/u_{\tau,g}; h_{\rm wm})$ to the DNS velocity fields, we can compute the marginal density function of the wall shear stress, which will later be used for comparison with the DNS wall shear stress,

$$p(\tau_w/\tau_{w,g}) = p(u_{\|,\rm wm}/u_{\tau,g})\frac{\mathrm{d}(u_{\|,\rm wm}/u_{\tau,g})}{\mathrm{d}(\tau_w/\tau_{w,g})}, \tag{1}$$

where the velocity distribution is directly from the DNS. In the *a priori* tests, the near-wall data is from the instantaneous channel flow with $Re_\tau = 1000$. The matching point location of the wall model is fixed at $h^+_{\rm wm} = 23.78$, which is an available wall-normal location in the DNS dataset that is close to the matching point location in the *a posteriori* tests in Sec. 2.2. This is close to the minimum matching point location for wall-modeled LES.

In the algebraic equilibrium wall model, the near-wall velocity profile follows the log law, which is expressed as

$$u^+ = \frac{1}{\kappa}\log(y^+) + B, \tag{2}$$

where the superscript + indicates that the variables are in the wall unit, y is the distance from the wall, κ is the von Kármán constant, and B is a constant. By assuming that the stress is normalized by ρ, the wall shear stress $\tau_w = u_\tau^2$ can be computed by solving

$$\frac{\|\mathbf{u}_{\|,\rm wm}\|}{u_{\tau,g}} = \frac{u_\tau}{u_{\tau,g}}\left[\frac{1}{\kappa}\log\left(\frac{h_{\rm wm}}{h}Re_\tau\frac{u_\tau}{u_{\tau,g}}\right) + B\right], \tag{3}$$

where h is the half-channel height, ν is the molecular viscosity, and the Reynolds number is $Re_\tau = u_{\tau,g}h/\nu$.

In the ODE equilibrium wall model, the wall shear stress is computed by a turbulent viscosity ν_T using the Prandtl mixing length model,

$$(\nu + \nu_T)\frac{du_\|}{dy} = \tau_w, \quad \nu_T = l_m u_\tau \mathcal{D}(y^+) = \kappa y u_\tau \mathcal{D}(y^+), \tag{4}$$

where $\mathcal{D}(y^+)$ is the van Driest damping function, and $l_m = \kappa y$ is the Prandtl mixing length. Therefore, the wall shear stress can also be computed by solving

$$\frac{d\left(\dfrac{\|\mathbf{u}_\|\|}{u_{\tau,g}}\right)}{d\left(\dfrac{y}{h}\right)} = \frac{Re_\tau\left(\dfrac{u_\tau}{u_{\tau,g}}\right)^2}{1 + \kappa\dfrac{y}{h}Re_\tau\dfrac{u_\tau}{u_{\tau,g}}\mathcal{D}\left(\dfrac{y}{h}Re_\tau\dfrac{u_\tau}{u_{\tau,g}}\right)}, \tag{5}$$

where $\|\mathbf{u}_\|\|/u_{\tau,g}$ satisfies the Dirichlet boundary conditions, both at the wall and at the matching point location.

At a fixed matching point $h^+_{\rm wm} = 23.78$ of a wall model, the $(u_{\|,\rm wm}/u_{\tau,g})$–$(\tau_w/\tau_{w,g})$ relation is shown in Fig. 1 (a) as the solid lines. The linear approximation of the wall model is indicated by the dashed lines with the 5% uncertainty level shown in the shaded areas. The model exhibits a nearly linear behavior within a relatively wide range. This is supported by the DNS dataset as shown in Fig. 1 (b). The major distribution range that stress and velocity lie in, which is visualized by the joint p.d.f., shows approximately linear behavior in the wall models, represented by the lines. Therefore, the global mean of the local wall shear stresses, determined by the wall models in the local wall unit, follows the wall-modeled mean wall shear stress in the global wall unit, i.e., $\overline{g(u_{\|,\rm wm}/u_{\tau,g}; h_{\rm wm})} \approx g(\overline{u_{\|,\rm wm}}/u_{\tau,g}; h_{\rm wm})$. This is not necessarily true if the linear approximation of the wall model does not hold. The wall models examined here are both convex functions. By using Jensen's inequality, we can prove that a strongly nonlinear wall model could greatly underestimate the global mean wall shear stress when the wall models are applied locally. However, the joint p.d.f. of the wall shear stress and the velocity $p(\tau_w/\tau_{w,g}, u_{\|,\rm wm}/u_{\tau,g})$ cannot be well represented when using the deterministic relationship between the stress and the velocity. To

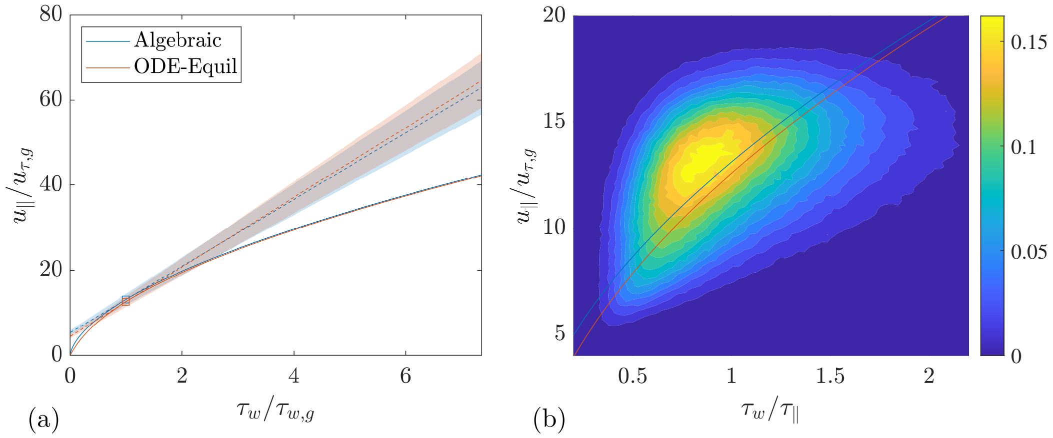

Figure 1: (a) The $(u_{\parallel,\mathrm{wm}}/u_{\tau,g})$–$(\tau_w/\tau_{w,g})$ relation for a fixed matching location $h^+_{\mathrm{wm}} = 23.78$ from two wall models are given by the solid lines. The global mean values are indicated by the hollow squares. The linear approximation of the wall model and the corresponding 5% uncertainty are indicated by the dashed lines and the shaded areas. (b) The joint p.d.f. of $\tau_w/\tau_{w,g}$ and $u_{\parallel,\mathrm{wm}}/u_{\tau,g}$ from DNS data shown by the contour. The wall model relations are superimposed on top as lines, which are the same relationship as (a).

be precise, without additional processing, the wall modeled data always falls on the lines in Fig. 1 (b), which has a totally different distribution from the DNS data. Therefore, the marginal density function of the wall shear stress does not necessarily preserve the distribution as in DNS. This is verified by Fig. 2 (a), where the DNS wall shear stress is indicated by the blue solid line. The distribution of the wall modeled stress computed from the DNS instantaneous velocity in the *a priori* tests is indicated by the dashed lines. They match mean wall shear stresses with the DNS. However, the distribution of the DNS wall shear stress has a smaller peak value and a heavier tail, which implies a higher chance of extreme wall shear stress events [21], compared to wall modeled data.

Though not shown here, these *a priori* tests have been carried out for a wide range of matching locations h_{wm}, and they provide similar conclusions. Therefore, when assuming that a universal mean velocity profile locally applies to the instantaneous profiles, wall models will in general provide an accurate mean velocity prediction at wall model matching locations. However, other statistics are not necessarily accurate in wall modeling. This reasons filtering the near-wall velocity before applying a wall model as it partially decorrelates the wall shear stress and the near-wall velocity without modifying the mean velocity.

2.2 A posteriori experiments

In order to study the interaction between a wall model and the LES solver, I carried out some wall-modeled LES simulations as the *a posteriori* tests. The LES solver used is LESGO, an in-house code developed and widely used for applications in the atmospheric boundary layer, rough walls, and wind turbines [22–24]. Wall-modeled LES simulations are conducted for turbulent channel flow with half-channel height h, at different Re_τ. The solver is pseudospectral in the longitudinal and spanwise directions, and uses second-order finite differencing in the wall-normal direction y. Therefore, the matching point location is at $\Delta y/2$ due to the staggered grid. The domain is $L_x = 2\pi h$ in the streamwise direction, and $L_z = 2\pi h$ in the spanwise direction. It is periodic in the streamwise and spanwise directions. A comparison between the full channels and the half channels does not reveal a significant difference in the statistics, so here only full-channel results are shown to reveal potentially large structures that cross the centerline. The subgrid-scale (SGS) model is the Lagrangian scale-dependent model [19], and the wall model is the algebraic model as detailed in Sec. 2.1. The details of the *a posteriori* tests are given in Table 1. The results are compared between tests with and without filtering the near-wall velocity at scale 2Δ, indicated by the suffix '-filt', where Δ is the wall-parallel grid size.

In Fig. 3 (a), I show the comparison of the mean velocity profiles from the wall-modeled LES for different Reynolds numbers and for whether the near-wall velocities are filtered or not. In the *a posteriori* experiments, all the mean velocities at the matching point locations provide the accurate prediction as

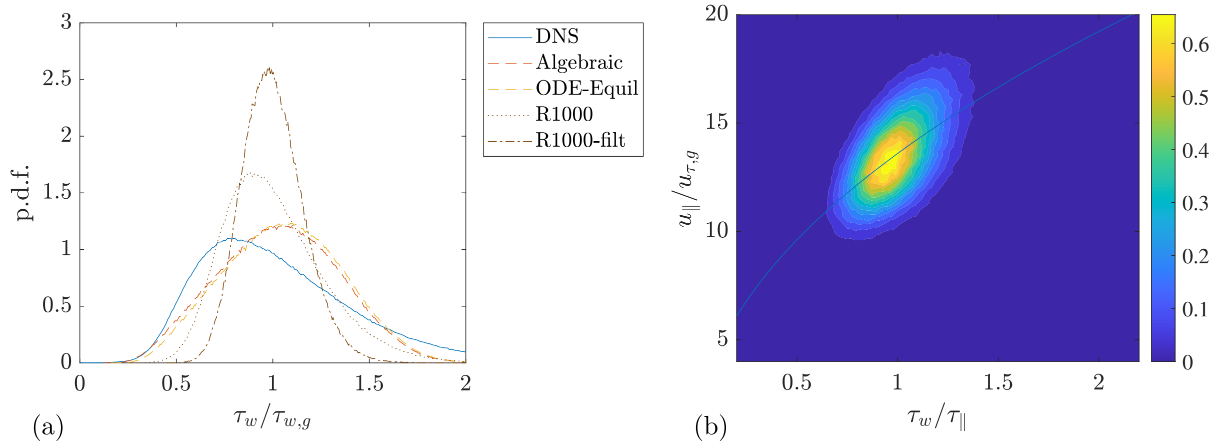

Figure 2: (a) The distribution of the DNS wall shear stress for $Re_\tau = 1000$ is given by the blue solid line. The wall shear stress predicted from the DNS velocity at $h_{\rm wm}$ by the algebraic wall model and the ODE equilibrium wall model are given by the orange and yellow dashed lines, respectively. The wall shear stress predicted from the wall-modeled LES using the algebraic wall model, both without and with filtering the near-wall velocity, is given by the dotted line and the dashed-dotted lines, respectively. (b) The joint p.d.f. of $\tau_w/\tau_{w,g}$ and $u_{\parallel,\rm wm}/u_{\tau,g}$ from wall-modeled LES data with filtering of the near-wall velocity. The wall model relation used in the *a posteriori* tests is superimposed on top of the contour as the blue solid line.

Case	Re_τ	N_x	N_y	N_z	$h^+_{\rm wm}$	Filter
R1000	1000	32	32	32	31.25	No
R1000-filt	1000	32	32	32	31.25	Yes
R2000	2000	64	64	64	31.25	No
R2000-filt	2000	64	64	64	31.25	Yes
R5200	5200	64	64	64	81.25	No
R5200-filt	5200	64	64	64	81.25	Yes

Table 1: The simulation details of the wall-modeled LES for turbulent channel flows. The results are labeled according to the Reynolds number and whether the near-wall velocities are filtered before applying the wall model.

expected from the algebraic wall model, and this aligns with the *a priori* results in Sec. 2.1. However, the velocity profiles beyond the matching point for the simulations without filtering the near-wall velocities consistently show a mismatch for all the Re_τ. This is an infamously persistent issue of wall modeling, known as 'log-layer mismatch' [18]. Some of the resolutions to the mismatch include filtering the near-wall velocity, using the third grid point as the matching location, and applying extra forcing or augmented eddy viscosity near the wall [18, 19, 25, 26]. The reasoning behind this is that the potentially underestimated wall shear stress of a wall model shifts the velocity profile upward, so these resolutions are intended to correctly predict the wall shear stress. Note that in Sec. 2.1, as long as the majority of the wall shear stress distribution lies in the linear range of a wall model, the wall model is capable of predicting the global mean. Therefore, the matching point locations actually provide the accurate velocities. However, the lack of accurate momentum transfer leads to inaccurate velocity profiles beyond the matching point locations. The key to a correct velocity profile, both at the matching point location and beyond, is the interaction between the wall model and the LES solver. Its impact on momentum transfer will be further elaborated in Sec. 2.3.

To understand the impact of the interaction between the wall model and the LES solver on the near-wall statistics, I compare wall modeling with and without filtering the near-wall velocity. Note that this analysis still falls within the range of quantifying the statistics. Though it does not directly validate whether the modeled physics is actually correct, the analysis can provide some possibilities. In Fig. 2 (b), I show the joint p.d.f. of $\tau_w/\tau_{w,g}$ and $u_{\parallel,\rm wm}/u_{\tau,g}$ from wall-modeled LES data with filtering of the near-wall velocity. The corresponding p.d.f. without filtering the near-wall velocity directly follows the line so

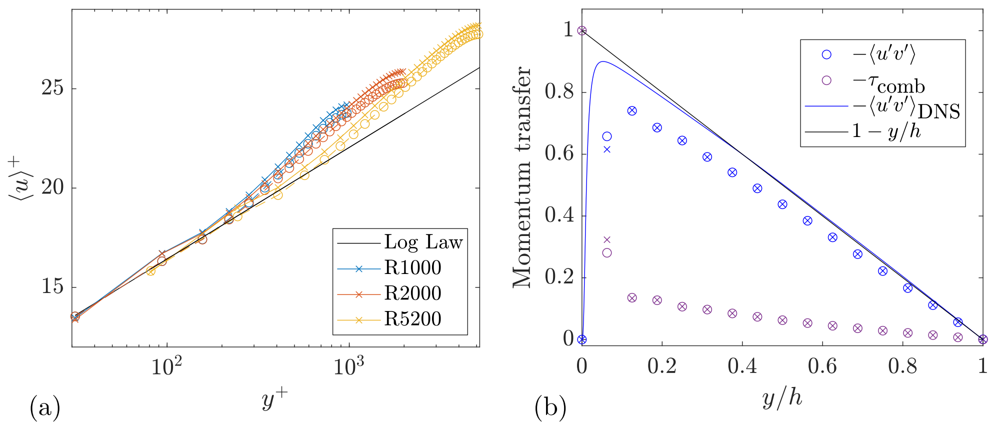

Figure 3: The *a posteriori* wall-modeled LES simulation results. (a) The mean velocity profiles of wall-modeled LES, compared with the log law indicated by the solid black line. The results without filtering the velocities are shown by the solid lines with crosses, while those with filtering the velocities are shown by the dashed lines with circles. The channel flows with $Re_\tau = 1000, 2000$ and 5200 are represented by the blue, the orange, and the yellow lines, respectively. (b) The decomposition of momentum transport for $Re_\tau = 1000$ wall-modeled LES is compared between R1000 and R1000-filt, which are represented by the crosses and the circles, respectively. The Reynolds stress in the DNS momentum transport is shown by the solid blue line for comparison. $1 - y/h$ is given by the black solid line. The contribution of the Reynolds stress is shown by the bright blue symbols or the blue line, while the contribution of τ_{comb} is shown by the purple symbols. All the quantities for momentum transfer are normalized by $\tau_{w,g} = u_{\tau,g}^2$.

it is not shown here. As seen in the contour, additional filtering decorrelates the wall shear stress and the velocity due to the mapping imposed by the wall model. Compared to the DNS behavior in Fig. 1, the distribution is strongly distorted, with the peak shifted and a lack of skewness. In the marginal density function for the wall shear stress shown in Fig. 2 (a), after the interaction with the SGS model, the R1000 shows more skewness than the original algebraic model. However, with filtering the near-wall velocity, the distribution is further distorted, with a lower standard deviation and a thinner tail. This indicates that filtering the near-wall velocity is another statistical resolution rather than providing the correct underlying turbulent structures. Otherwise, the distribution should show a closer match to the DNS. The structures will be further extracted and compared in Sec. 2. The challenge of a statistical resolution is its lack of generalizability. The fixed flow behavior could be case-specific and solver-dependent. In Fig. 3 (a), cases with different Reynolds numbers have different levels of mismatch and also differ from [18], which used a different solver. After filtering, R5200-filt has a slightly underestimated velocity at the third grid point. Therefore, filtering is not the final solution for an accurate mean profile.

2.3 Momentum transfer

As illustrated in the previous sections, a wall model is usually capable of providing an accurate prediction of the velocity at the matching point location. However, the interaction between the wall model and the LES solver prevents the correct momentum transfer in the wall-modeled LES, resulting in inaccurate velocity profiles beyond the matching point. To quantify the momentum transfer, we can start with the streamwise momentum equation,

$$\frac{\partial u}{\partial t} + u_i \frac{\partial u}{\partial x_i} = -\frac{1}{\rho}\frac{\partial p}{\partial x} + \nu \frac{\partial^2 u}{\partial x_i \partial x_i} + \frac{\partial}{\partial x_i}\left[\nu_T \left(\frac{\partial u}{\partial x_i} + \frac{\partial u_i}{\partial x}\right)\right], \tag{6}$$

where the subscript $i = 1, 2, 3$ refers to the streamwise, wall-normal, and spanwise directions. Here, I explicitly apply the eddy-viscosity SGS model for simplicity. After averaging in the streamwise and spanwise directions, and integrating in the vertical direction from the wall to the matching point h_{wm}, the integrated streamwise momentum equation is

$$\overline{u'v'} = -\frac{1}{\rho}\frac{\partial p}{\partial x} h_{\text{wm}} + \overline{(\nu + \nu_T)\frac{\partial u}{\partial y}} - \tau_{w,g}, \tag{7}$$

Journal of Physics: Conference Series **3230** (2026) 012023 doi:10.1088/1742-6596/3230/1/012023

where overline $\bar{\cdot}$ indicates the spatial and temporal averaging. By using the balance between the pressure gradient and the wall shear stress, the momentum transfer purely depends on the Reynolds stress, i.e.,

$$u_{\tau,g}^2\left(1-\frac{h_{\mathrm{wm}}}{h}\right)\approx-\overline{u'v'}+(\nu+\overline{\nu_T})\frac{\partial U}{\partial y}\triangleq-\overline{u'v'}+\tau_{\mathrm{comb}}. \tag{8}$$

The momentum transfer is thus decomposed into the Reynolds stress, viscous stress and SGS stress. The combination of the viscous stress and the SGS stress is indicated by τ_{comb}. The SGS model is not necessarily of the eddy-viscosity type, but it typically provides an estimation of momentum transfer based on the velocity gradient $\partial u/\partial y$. For simplicity, the eddy-viscosity model is considered to explicitly provide the relationship between the velocity profile and the momentum transfer.

In Fig. 3 (b), the decomposition of the Reynolds stress and the combined stress is compared between the DNS solution and the wall-modeled LES solutions with and without filtering the near-wall velocity for $Re_\tau = 1000$. The LES solutions typically underestimate the Reynolds stress, and thus the SGS stress estimates the difference to ensure correct momentum transfer. However, in the near-wall region, the interaction between the wall model and the SGS model leads to a difference between cases whether the velocity is filtered or not. This interaction has not received enough attention yet, though some literature already shows that wall-modeled LES is highly sensitive to the SGS model [6, 27, 28].

In the simulation without velocity filtering, the insufficient momentum transfer at the matching point leads to an abnormally high velocity gradient. Even when the wall shear stress is correctly imposed, the velocity profile after the matching point shifts upwards, leading to the 'log-layer mismatch'. When the near-wall velocity is filtered, the Reynolds stress is higher, and thus the velocity profile is more accurate, as shown in Fig. 3 (a). This situation can also be resolved by modifying the SGS model near the wall. This also explains why augmenting the eddy viscosity at the wall in some wall-modeled LES performs better than simply imposing the wall shear stress [26]. However, further investigation is needed to understand how other resolutions, including using a grid point further off the wall as the matching location, can help achieve the correct interaction between the wall model and the LES solver. Similar discussions could be made for complex flows, such as flows with pressure gradient, and flows with rotation, etc, which are beyond the scope of this work.

3 Contribution of momentum-transfer structures

In the previous section, we see how momentum transfer impacts the velocity profile prediction of wall-modeled LES. Accurate momentum transfer is an important component of the interaction between the wall model and the SGS model. Therefore, I will discuss the impact of structures in a channel flow that are closely related to the momentum transfer [29].

I focus on the Qs structures, which are connected regions satisfying

$$|-u'(\mathbf{x})v'(\mathbf{x})|>Hu_{\mathrm{rms}}(y)v_{\mathrm{rms}}(y), \tag{9}$$

where $u_{\mathrm{rms}}(y)$ and $v_{\mathrm{rms}}(y)$ are the root mean square (r.m.s.) of the streamwise and wall-normal velocities at the corresponding wall-normal location y. $H = 1.75$ is the detection threshold for the hyperbolic-hole size. The Q2 events (ejection) with $u < 0, v > 0$ and the Q4 events (sweep) with $u > 0, v < 0$ are considered major contributors to the Reynolds stress in the DNS channel flows, especially the attached events [29]. Therefore, they are referred to as Q^- events, and here, they are examined in the wall-modeled LES. The details of the Qs event identification can be found in [29].

Fig. 4 (a) shows a typical large Qs structure in a wall-modeled LES. It turns out that large Qs structures in the wall-modeled LES are mostly Q2 events. They are typically long in the streamwise direction and easily cross the domain center in the wall-normal direction. Though "relatively few (25-30% by number), large and intense wall-attached Q^-s are responsible for most of the momentum transfer" in DNS simulations [29], the wall-modeled LES exhibits a fairly different behavior. If the structures contain the volume in the wall-model area, I consider them as wall-attached, similar to the original definition that requires $y^+_{\mathrm{min}} < 20$ for each object. Only 6.7% of the Qs structures are attached Qs events, and they contribute relatively little to the momentum transfer, especially in the near-wall region.

In Fig. 4 (b), the total Reynolds stress is shown as the solid line, which is a major contribution of the momentum transfer beyond the wall modeling region. However, the Q2 and Q4 events only contribute to a small portion of the total Reynolds stress, and that contribution decreases with the wall-normal distance. Q4 events contribute relatively closer to the wall than Q2 events. In general, they do not contribute as much as the DNS results, especially in the near-wall region. This seems to be related to the lack of wall-attached events. Moreover, the Qs structures are contributing almost zero to the SGS stress

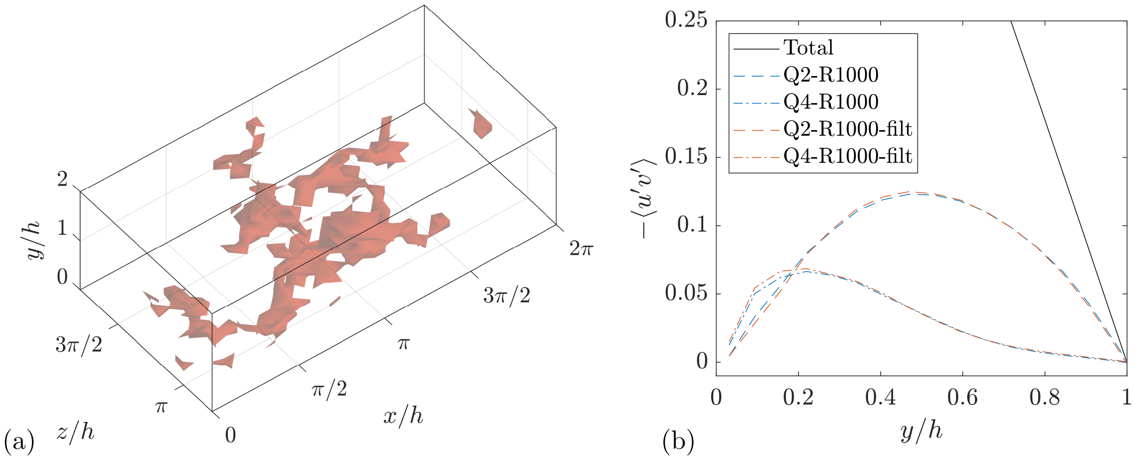

Figure 4: (a) A typical large Qs structure observed in the instantaneous flow field. Here, we have a Q2 event in R1000-filt. (b) The contribution of the Qs structures to the Reynolds stress. The total Reynolds stress is shown as the solid line. The contribution of the Q2 structures is shown by the dashed lines, while the contribution of the Q4 structures is shown by the dashed-dotted lines. The comparison between R1000 and R1000-filt is given by the orange lines and the blue lines, respectively.

term, so such a comparison is not plotted, which indicates that the Qs structures are irrelevant to the SGS model. If we regard LES solutions as projected DNS solutions on the LES state space, it is possible that the momentum-transfer structures are obscured due to the projection, which might require modifying the detection threshold H for LES solutions. This requires further study in both the *a priori* and *a posteriori* tests. However, the diminishing wall-attached events might indicate missing underlying physics in wall modeling, and thus, momentum transfer could be solely a statistical fitting of the high-resolution data. This justifies the statistical approaches to modeling discrepancies, such as the 'log-layer mismatch'.

In Fig. 5, I further show the pre-multiplied distribution of the Qs structures with respect to their volume. It is clearly shown that Q4 events make up a much smaller portion and are generally smaller structures. Though the majority of the Q2 structures are not attached to the wall, they are not far from the wall. It is postulated that because the wall model modifies the distribution of the wall shear stress and the wall-parallel velocity, the wall-attached Qs structures are not easy to formulate in the near-wall region. Therefore, accurate momentum transfer is not determined by the Qs structures in wall-modeled LES, even though they are the significant momentum-transfer structures in DNS.

Further, comparing the wall-modeled LES with and without filtering the near-wall velocity, almost no difference is observed in Qs events when their mean velocity profiles differ. In Fig. 4 (b), the Q2 and Q4 events are contributing similarly to the Reynolds stress for both simulations. In Fig. 5, the distribution of the Q2 and Q4 events regarding their volume is almost the same. This further verifies that the filtering technique does not necessarily modify the prediction of momentum-transfer structures as Qs events. The filtering tunes the minor events that are below the threshold, which also contributes to the momentum transfer.

4 Conclusion and future work

In this work, I explore the modeled turbulence in a wall-modeled LES. Due to the chaotic nature of turbulence and the complex coupling between a wall model and the LES solver, the wall-modeled LES is typically only developed and evaluated from a statistical perspective, and they are often applicable only within a limited range. In order to understand how the limitations of a wall model are imposed through wall turbulence, both the *a priori* and the *a posteriori* tests are carried out. As expected, as long as the majority of the wall shear stress distribution lies in the linear range of a wall model, the wall model is capable of predicting the global mean. This is true for both in the *a priori* tests and the *a posteriori* tests, where the velocity profile at the matching point is accurate. However, in the *a posteriori* tests, the interaction between the wall model and the LES solver may not necessarily provide the correct momentum transfer, and thus may predict an inaccurate velocity profile beyond the matching point.

To examine how momentum is transferred in modeled turbulence, I decompose the momentum transfer into the Reynolds stress, viscous stress and SGS stress. Whether or not filtering the near-wall velocity in

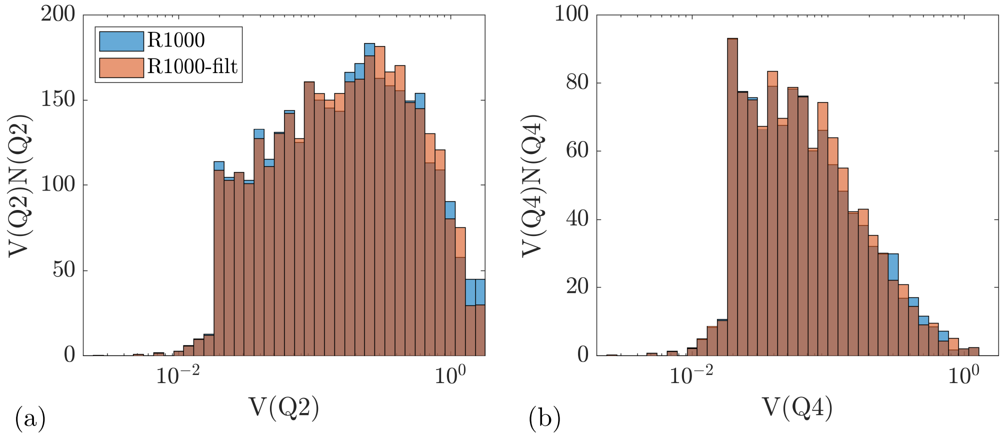

Figure 5: The pre-multiplied distribution of the Qs structures with respect to their volume. Here, V(·) is the volume of the structure, and N(·) is the number of the structures. (a) Q2 structures. (b) Q4 structures. The comparison between the R1000 and R1000-filt is shown by the blue blocks and the orange blocks, respectively.

a wall-modeled LES is used as an example to show how wall models are developed and optimized for an accurate momentum transfer prediction. It turns out that the filtering tunes the Reynolds stress at the matching point, and thus resolves the issue of 'log-layer mismatch'. However, further investigation shows that the modeled near-wall turbulence contains few wall-attached Qs events, and thus lacks the major structures that contribute to the momentum transfer. Filtering does not change the behavior of the Qs events, and how it modifies the events below the detection threshold requires further investigation. It is possible that a direct comparison with the DNS dynamics does not apply to the LES since the LES solution space is actually a projection of the DNS solution space. The projection is typically considered as applying a filter to the DNS solutions, but it is not discussed here since the accurate projection for an LES solution is still controversial [2, 30]. The results could be highly sensitive to the choice of solution space projection, i.e., the filter type. More work is needed to understand the resolvable physical structures in wall-modeled turbulence. With that, the generalizability of wall models could be extended due to their physical foundation.

In model applications, if the underlying physics is better represented, the higher-order statistics and the instantaneous structures of wall-modeled LES will become more valuable. For example, when the joint p.d.f. of wall shear stress and velocity is better predicted by a wall model, wall-modeled LES can not only predict the mean profiles, but also capture extreme shear stress events, which could be useful in real-world applications. The physical generalizability could also assist in developing a wall model to handle extended parameter space, such as high Reynolds numbers, and extended physical processes, such as flows with a non-zero pressure gradient. However, it is also challenging to involve such physical knowledge in actual model development, because the observed structures require extra stencil points. This will pose further challenges to model implementation and impose further limits on model application. Therefore, we need to strike a balance between simplicity and accuracy.

5 Acknowledgement

This work was partially supported by the European Research Council under the Caust grant ERC-AdG-101018287, and XH was partially supported by the 3CRS Project (NSF OIA 2316271). XH would like to thank Dr. Peng Chen for providing the code to identify the Qs structures and for the insightful discussion.

References

[1] Moin P and Mahesh K 1998 *Annu. Rev. Fluid Mech.* **30** 539–578
[2] Langford J A and Moser R D 1999 *J. Fluid Mech.* **398** 321–346
[3] Maeyama H and Kawai S 2023 *J. Fluid Mech.* **969** A29
[4] Duprat C, Balarac G, Métais O, Congedo P M and Brugière O 2011 *Phys. Fluids* **23**
[5] Huang X L, Yang X I and Kunz R F 2019 *Phys. Fluids* **31** 125105

Journal of Physics: Conference Series **3230** (2026) 012023 doi:10.1088/1742-6596/3230/1/012023

[6] Park G I 2017 *AIAA J.* 3709–3721
[7] Giometto M G, Lozano-Duran A, Park G I and Moin P 2017 *Cent. for Turbul. Res. Annu. Res. Briefs* 193–205
[8] Zhou D and Bae H J 2024 *J. Comput. Phys.* **506** 112948
[9] Monty J P, Harun Z and Marusic I 2011 *Int. J. Heat Fluid Flow* **32** 575–585
[10] Bobke A, Vinuesa R, Örlü R and Schlatter P 2017 *J. Fluid Mech.* **820** 667–692
[11] Hayat I and Park G I 2024 *AIAA J.* **62** 557–572
[12] Iyer P S and Malik M R 2019 *Phys. Rev. Fluids* **4** 074604
[13] Maronga B, Gryschka M, Heinze R, Hoffmann F, Kanani-Sühring F, Keck M, Ketelsen K, Letzel M O, Sühring M and Raasch S 2015 *Geoscientific Model Development* **8** 2515–2551
[14] Bose S T and Park G I 2018 *Annu. Rev. Fluid Mech.* **50** 535–561
[15] Goc K A, Lehmkuhl O, Park G I, Bose S T and Moin P 2021 *Flow* **1** E14
[16] Lozano-Durán A and Bae H J 2023 *J. Fluid Mech.* **963** A35
[17] Garmann D J, Schwartz M J, Larsson J, Bermejo-Moreno I, Uzun A, Ganju S, Brehm C, Mukha T, Parsani M, Flad D *et al.* 2024 Summary of the wall-modeled les test suite from the 2024 AIAA high-fidelity CFD verification workshop *AIAA Aviation Forum and Ascend 2024* p 3697
[18] Kawai S and Larsson J 2012 *Phys. Fluids* **24** 015105
[19] Bou-Zeid E, Meneveau C and Parlange M 2005 *Phys. Fluids* **17** 025105
[20] Li Y, Perlman E, Wan M, Yang Y, Meneveau C, Burns R, Chen S, Szalay A and Eyink G 2008 *J. Turbul.* N31
[21] Yang X I A, Hong J, Lee M and Huang X L D 2021 *Phys. Rev. Fluids* **6**(5) 054603
[22] Porté-Agel F, Meneveau C and Parlange M B 2000 *J. Fluid Mech.* **415** 261–284
[23] Anderson W and Meneveau C 2011 *J. Fluid Mech.* **679** 288–314
[24] Shapiro C R, Gayme D F and Meneveau C 2018 *J. Fluid Mech.* **841** R1
[25] Yang X I, Park G I and Moin P 2017 *Phys. Rev. Fluids* **2** 104601
[26] Bae H J and Lozano-Durán A 2021 *Fluids* **6** 112
[27] Rezaeiravesh S, Mukha T and Liefvendahl M 2019 *Comput. Fluids* **185** 34–58
[28] Whitmore M, Lozano-Durán A and Moin P 2020 *arXiv preprint arXiv:2012.14900*
[29] Lozano-Durán A, Flores O and Jiménez J 2012 *J. Fluid Mech.* **694** 100–130
[30] Huang X, Leung S, Whitmore M, Elnahhas A and Bae H 2024 Consistent data-driven subgrid-scale model development for large-eddy simulation *Proc. of the Summer Program* pp 395–404